ELSEVIER

Engineering Analysis with Boundary Elements 25 (2001) 31–40

ENGINEERING ANALYSIS *with* BOUNDARY ELEMENTS

www.elsevier.com/locate/enganabound

Stress analyses around holes in composite laminates using boundary element method

E. Pan[a,*], B. Yang[a], G. Cai[a], F.G. Yuan[b]

[a]*Structures Technology, Inc., 543 Keisler Dr., Suite 204, Cary, NC 27511, USA*
[b]*Department of Mechanical and Aerospace Engineering, North Carolina State University, Raleigh, NC 27695, USA*

Received 9 February 1999; revised 22 May 1999; accepted 24 August 2000

Abstract

A three-dimensional (3D) boundary element method (BEM) is developed for the analysis of composite laminates with holes. Instead of using Kelvin-type Green's functions of anisotropic infinite space, 3D layered Green's functions with the materials of each layer being generally anisotropic, derived recently in the Fourier transform domain, are implemented into a 3D BEM formulation. A novel numerical algorithm is designed to calculate layered Green's functions efficiently. It should be noted that since layered Green's functions satisfy exactly the continuity conditions along the interfaces and top and bottom free surfaces a priori, the model becomes truly 2D and discretization is only needed along the hole surface and prescribed traction and/or displacement boundaries. To test the validity and accuracy of the proposed method, the present layered BEM formulation is applied to the problem of an infinite anisotropic plate with a circular hole where the analytical solution is available. It is found that even with a very coarse mesh, the present BEM can predict the hoop stress very accurately along the hole surface. The BEM formulation is then applied to analyze two composite laminates $(90/0)_s$ and $(-45/45)_s$, under a remote in-plane strain, that have been studied previously with different approaches. For the $(90/0)_s$ case, the hoop stresses along the hole surface predicted by the present layered BEM formulation are in very close agreement with the previous results. For the $(-45/45)_s$ case, however, it is found that a nearly converged solution (less than 5% convergence by doubling the mesh) by the present method is at significant variance with the previous ones that are lack-of-convergence checks. It can be expected that for designing the bolted joints of composites with many layers, a computational tool developed based on the present techniques would be robust and offer a much better solution with regard to accuracy, versatility and design cycle time.

Keywords: Boundary element method; Composite laminates with holes; Layered Green's functions

1. Introduction

In the design of aircraft structures using composites, the structural components must be joined by fastening or bonding for transferring load. Each technique has its own advantages and limitations [11,22]. For example, many components of the aircraft must be arranged so that they can be disassembled for shipping, inspection, repair, or replacement. Fasteners are usually used to join such components. However, the weight advantages of composite structures are frequently eroded by using mechanical fasteners. Adhesive bonding provides a desirable alternative to mechanical fasteners in composite structures.

Joints are perhaps the most common source of failure in aircraft structures and therefore it is important that all aspects of joint design are given consideration during the structural design. Joining metallic structures is a well-developed technology. However, advanced composite joints introduce design concepts different from those common to metal construction [7] because of low strain capability, inhomogeneity, and anisotropy and thus exhibit complex failure modes. Although industry and government research agencies have been investigating the joining of composites, and some of the data and testing methods have been established in MIL-HDBK-17 and in the Advanced Composite Design Guide, current capability to predict failure strength is less than adequate.

Joint failures result from stress concentrations, secondary stresses due to eccentricities, or a combination of both. Failure of bolted joints usually begins at locations immediately adjacent to the contact points of bolts and laminates where enhanced stress concentrations render fastener holes more susceptible to crack initiation. These cracks represent the most common origin of structural failures in aircraft. Therefore, to fully develop the analytical design procedures of

* Corresponding author. Tel.: +1-919-816-0434; fax: +1-919-816-0438.
E-mail address: pan@ipass.net (E. Pan).

0955-7997/01/$ - see front matter
PII: S0955-7997(00)00066-7

advanced composites in weight-critical aircraft structures, an accurate assessment of the stresses for joints, either fastened or bonded under general loading conditions with these failure modes, is essential for reliable strength evaluation and failure prediction.

Considerable effort has been made to investigate the failure of bolted joints in the last two decades. A large body of experimental data has been generated. Three possible ultimate in-plane failure modes, namely bearing, shear-out, and tension, have been clearly identified. A positive influence on strength due to lateral constraint, thereby clamping forces, has been demonstrated by numerous researchers (e.g. Refs. [24,3,6]). Stacking sequence and ply orientation [3,17,6], and geometrical factors of clearance-fit oversize hole, hole diameter (D), laminate thickness(h) and width (W), and edge distance (e), e.g. D/h, W/D, e/D ratios, have been documented [9,5]. Stress analyses around a bolted hole have been conducted using boundary layer solutions [25,26], anisotropic elasticity solution [4,19], linear laminate finite element methods (FEMs) [23,31], 3D discrete layer FEM [20,21,13,18], and spline variational method [8].

Despite research on the failure of joints, the fundamental physics and the basic mechanics principles of the failure process have remained largely inaccessible. These engineering approaches to strength prediction are mainly phenomenological, i.e. empirical strength characterization data with only indirect association were established between the true representation and the physics or mechanics of the failure process. The damage adjacent to the holes, which affects the stress redistribution and leads to the ultimate failure, has been neglected. Since the failure of joints is clearly a 3D phenomenon, it is obvious that, to be useful in predicting failure, an accurate 3D stress analysis, including the damage along the curved bolted boundary, is required.

The FEM has experienced a tremendous growth in composite structural design. It is known as one of the 'domain'-type techniques in which discretizations are introduced in the whole domain. An alternative way to solve composite structural problems is by using the boundary element method (BEM) which discretizes the boundary of a problem only. This technique is developed based on a transformation of the governing partial differential equations, which involve unknown fields inside and on the boundary of a domain, into an integral equation involving fields on the boundary only. In recent years, the BEM technique has been gaining increasing popularity among the numerical methods. The advantages of a BEM over a domain-based method include:

1. reduced problem dimensionality by one;
2. smaller amount of computer storage requirement;
3. no discretization error inside the domain;
4. accurate stress prediction for stress concentration problems.

However, the *traditional* BEM formulation has its limitations when applied directly to a multilayered composite structure with damage, due to certain inherent deficiencies associated with this type of BEM formulation such as:

(a) the fundamental solution used is for full-space (i.e. Kelvin-type) Green's functions;
(b) because of (a), all interfaces between different layers need to be discretized;
(c) because of (b), the resulting system of algebraic equations may become very large for multilayered 3D composite structures, inhibiting a solution on the current PC computers.

To resolve these shortcomings, layered Green's functions that satisfy the interfacial conditions and hence eliminate the need for interface discretization need to be developed. Previously, various methods were proposed to derive Green's functions of this type (for a brief review, see Ref. [14]). Benitez and co-workers [1,2] attempted the implementation of one type of layered Green's functions into a BEM formulation.

In this paper, we present stress analyses of composite laminates with holes using a *non-traditional* BEM formulation. That is, instead of using full-space (Kelvin-type) Green's functions, layered Green's functions recently developed by Yuan and Yang [32] are implemented into our BEM formulation. These Green's functions are derived in the Fourier-transformed domain based on the Stroh formalism [27]. To obtain physical-domain Green's functions, an adaptive quadrature properly connected to the BEM formulation is proposed. Since the displacement and traction continuity conditions are exactly satisfied along the layer interfaces and the top and bottom free surfaces, discretization is only needed around the holes and on the prescribed traction and/or displacement boundaries. To check the accuracy and efficiency, our method is first applied to the problem where an infinite, homogeneous, and anisotropic plate with a circular hole is under a far-field stress. It is found that even with a very coarse mesh, the results obtained by our BEM formulation are very close to the exact solutions. The formulation is then applied to analyze two composite laminates $(90/0)_s$ and $(-45/45)_s$, with a central hole under a remote uniform in-plane strain. For the $(90/0)_s$ composite laminates, the hoop stresses along the hole surface predicted by the present layered BEM formulation are in very close agreement with the previous results. For the $(-45/45)_s$ composite laminates, however, it is found that a nearly converged solution (less than 5% convergence by doubling the mesh) by the present method differs significantly from the previous ones. The present method provides an accurate and efficient numerical tool that can be applied to more complicated problems where other methods may not be able to access with the current computer power.

2. 3D boundary element formulation

Consider a horizontally layered structure with each layer being homogeneous, anisotropic, and linearly elastic, bounded by an internal lateral surface S_{in}, an external lateral surface S_{ex}, a top surface S_t, and a bottom surface S_b. For such a structure, the internal displacement can be expressed by the following integral:

$$u_i(\mathbf{X}_p) + \int_S T^*_{ij}(\mathbf{X}_p, \mathbf{X}_s) u_j(\mathbf{X}_s)\, dS(\mathbf{X}_s) = \int_S U^*_{ij}(\mathbf{X}_p, \mathbf{X}_s) t_j(\mathbf{X}_s)\, dS(\mathbf{X}_s), \quad (1)$$

where u_j and t_j are the displacement and traction on the total boundary $S = S_{in} + S_{ex} + S_t + S_b$, and $U^*_{ij}(\mathbf{X}_p, \mathbf{X}_s)$ is the layered Green's displacement in i-direction at field point $\mathbf{X}_s$ caused by a point force in j-direction at source point $\mathbf{X}_p$. A similar definition holds for the layered Green's traction $T^*_{ij}(\mathbf{X}_p, \mathbf{X}_s)$. These Green's functions have been derived recently by Yuan and Yang [32] in the Fourier transform domain and a brief description will be given in the next section. In deriving Eq. (1), a zero body-force has been assumed for the sake of simplicity.

Let $\mathbf{X}_p$ approach a point $\mathbf{Y}_s$ on the boundary, we arrive at the boundary integral equation

$$b_{ij}(\mathbf{Y}_s) u_j(\mathbf{Y}_s) + \int_S T^*_{ij}(\mathbf{Y}_s, \mathbf{X}_s) u_j(\mathbf{X}_s)\, dS(\mathbf{X}_s) = \int_S U^*_{ij}(\mathbf{Y}_s, \mathbf{X}_s) t_j(\mathbf{X}_s)\, dS(\mathbf{X}_s), \quad (2)$$

where b_{ij} are coefficients that depend only upon the local geometry of the boundary at $\mathbf{Y}_s$. For a smooth boundary, $b_{ij} = 0.5\delta_{ij}$, in which δ_{ij} is the Kronecker delta. Discretizing the total boundary S with N nodal points and NE elements, Eq. (2) can then be reduced to a set of linear algebraic equations (for $i = 1, 2, \ldots, N$)

$$\{\mathbf{b}\}\{\mathbf{u}\}^i + \sum_{j=1}^{NE} \{\hat{\mathbf{H}}\}^{ij}\{\mathbf{u}\}^j = \sum_{j=1}^{NE} \{\mathbf{G}\}^{ij}\{\mathbf{t}\}^j, \quad (3)$$

where matrices $\{\hat{\mathbf{H}}\}$ and $\{\mathbf{G}\}$ are the integrals of the layered Green's traction and displacement on the generic element, i.e.

$$\hat{\mathbf{H}} = \int_{-1}^{1}\int_{-1}^{1} \mathbf{T}^*\mathbf{\Phi}|\mathbf{J}|\, d\xi_1\, d\xi_2 \quad (4)$$

$$\mathbf{G} = \int_{-1}^{1}\int_{-1}^{1} \mathbf{U}^*\mathbf{\Phi}|\mathbf{J}|\, d\xi_1\, d\xi_2. \quad (5)$$

In Eqs. (4) and (5), $\mathbf{\Phi}(\xi_1,\xi_2)$ is the shape function matrix and $\mathbf{J}(\xi_1,\xi_2)$ the Jacobian of the mapping from (x, y, z) to (ξ_1, ξ_2).

It is noteworthy that since the Green's displacement, $\mathbf{U}^*$, has only a weak singularity, the integral for $\mathbf{G}$ on the right-hand side of Eq. (5) can be easily carried out numerically. Although the right-hand side of Eq. (4) involves a Cauchy-type singularity, it can be treated by the rigid body motion method. At the same time, the calculation of $\{\mathbf{b}\}$ in Eq. (3) can be avoided [15]. Therefore, Eq. (3) can be arranged and solved for the unknown boundary values u_j and/or t_j. It is emphasized that since layered Green's functions satisfy exactly the displacement and traction continuities along the layer interfaces, discretization is only needed on the real problem boundaries, which therefore greatly reduces the problem size and increases the accuracy of the solution. Furthermore, if the top and bottom surfaces are traction free, which is the common situation in composite structure analysis, no discretization will be necessary on these two surfaces. Therefore, the only discretization needed is along the lateral internal and external surfaces, i.e. $S = S_{in} + S_{ex}$ in Eq. (2).

3. Green's functions for composite laminates

Green's functions in multilayered anisotropic plates have been derived recently by Yuan and Yang [32]. They are based on the Stroh formalism and 2D Fourier transforms. For the sake of easy description of the following sections, a brief presentation of Green's functions is given below.

Consider a composite laminate that consists of n horizontal layers of different anisotropic elastic materials (Fig. 1). Let a Cartesian coordinate system (x_1, x_2, x_3) be chosen such that the x_1–x_2 plane lies on the bottom surface of the laminate and the composite occupies $x_3 \geq 0$. Each layer of the laminate occupies the region $h_{j-1} \leq x_3 \leq h_j$, $j = 1, 2, \ldots, n$ with $0 = h_0 < h_1 < \cdots < h_n$. Along each interface $x_3 = h_j$ $(j = 1, 2, \ldots, n-1)$, the displacements and the tractions are continuous. The first step is to derive Green's functions in the Fourier-transformed domain with the transform being defined as

$$\tilde{\mathbf{u}}_k(y_1, y_2, x_3) = \int\int \mathbf{u}_k(x_1, x_2, x_3)\, e^{i\mathbf{y}\cdot\mathbf{x}}\, dx_1\, dx_2, \quad (6)$$

where $\mathbf{y} = (y_1, y_2)$ is the transform vector, $\mathbf{x}$ denotes (x_1, x_2), and $\mathbf{y}\cdot\mathbf{x} = y_1x_1 + y_2x_2$.

Assuming that the laminate is subjected to a concentrated force at a point (x_1^0, x_2^0, d) in the kth layer $(h_{k-1} < d < h_k)$ shown in Fig. 1, Green's functions (displacements and tractions on an (x_1,x_2)-plane) in the transformed domain were obtained, based on the Stroh formalism, as

$$\begin{aligned}
\tilde{\mathbf{u}}_m(y_1, y_2, x_3)\, e^{-i\mathbf{y}\cdot\mathbf{x}^0} &= i\eta^{-1}\bar{\mathbf{A}}_m\langle e^{-i\bar{p}_*^{(m)}\eta(x_3 - h_{m-1})}\rangle\bar{\mathbf{q}}_m \\
&\quad + i\eta^{-1}\mathbf{A}_m\langle e^{-ip_*^{(m)}\eta(x_3 - h_m)}\rangle\mathbf{q}'_m \\
\tilde{\mathbf{t}}_m(y_1, y_2, x_3)\, e^{-i\mathbf{y}\cdot\mathbf{x}^0} &= \bar{\mathbf{B}}_m\langle e^{-i\bar{p}_*^{(m)}\eta(x_3 - h_{m-1})}\rangle\bar{\mathbf{q}}_m \\
&\quad + \mathbf{B}_m\langle e^{-ip_*^{(m)}\eta(x_3 - h_m)}\rangle\mathbf{q}'_m
\end{aligned} \quad (7)$$

$m = 1, 2, \ldots, n$ and $m \neq k$

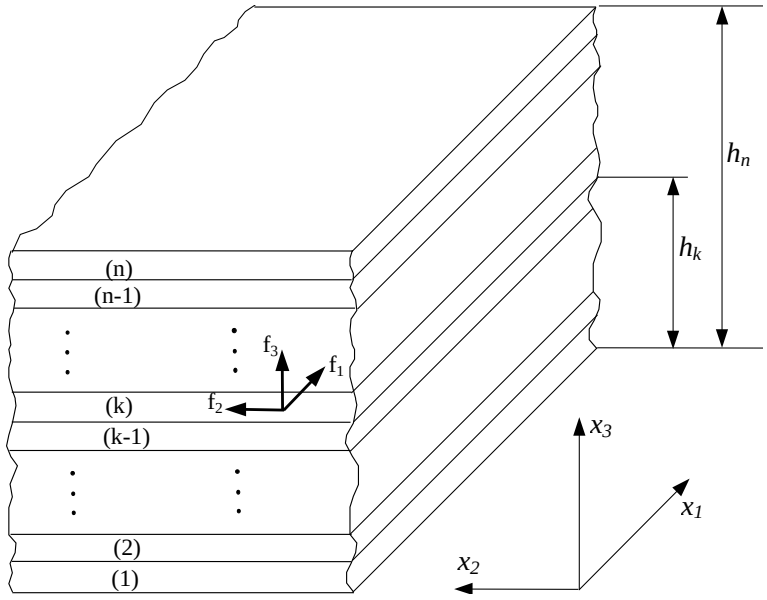

Fig. 1. A layered composite laminate under a point force acting at (x_1^0, x_2^0, d) in the kth layer.

for any layer $m \neq k$, and

$$\begin{aligned}\tilde{\mathbf{u}}_k(y_1,y_2,x_3)\,\mathrm{e}^{-\mathrm{i}\mathbf{y}\cdot\mathbf{x}^0} &= \mathrm{i}\eta^{-1}\mathbf{A}_k\langle \mathrm{e}^{-\mathrm{i}\bar{p}_*^{(k)}\eta(x_3-d)}\rangle\mathbf{q}^{\infty}\\ &\quad+\mathrm{i}\eta^{-1}\bar{\mathbf{A}}_k\langle \mathrm{e}^{-\mathrm{i}\bar{p}_*^{(k)}\eta(x_3-h_{k-1})}\rangle\bar{\mathbf{q}}_k\\ &\quad+\mathrm{i}\eta^{-1}\mathbf{A}_k\langle \mathrm{e}^{-\mathrm{i}p_*^{(k)}\eta(x_3-h_k)}\rangle\mathbf{q}_k'\end{aligned}\tag{8}$$

$$\begin{aligned}\tilde{\mathbf{t}}_k(y_1,y_2,x_3)\,\mathrm{e}^{-\mathrm{i}\mathbf{y}\cdot\mathbf{x}^0} &= \mathbf{B}_k\langle \mathrm{e}^{-\mathrm{i}p_*^{(k)}\eta(x_3-d)}\rangle\mathbf{q}^{\infty}\\ &\quad+\bar{\mathbf{B}}_k\langle \mathrm{e}^{-\mathrm{i}\bar{p}_*^{(k)}\eta(x_3-h_{k-1})}\rangle\bar{\mathbf{q}}_k\\ &\quad+\mathbf{B}_k\langle \mathrm{e}^{-\mathrm{i}p_*^{(k)}\eta(x_3-h_k)}\rangle\mathbf{q}_k'\end{aligned}$$

for $h_{k-1} \le x_3 < d$

$$\begin{aligned}\tilde{\mathbf{u}}_k(y_1,y_2,x_3)\,\mathrm{e}^{-\mathrm{i}\mathbf{y}\cdot\mathbf{x}^0} &= -\mathrm{i}\eta^{-1}\bar{\mathbf{A}}_k\langle \mathrm{e}^{-\mathrm{i}p_*^{(k)}\eta(x_3-d)}\rangle\bar{\mathbf{q}}^{\infty}\\ &\quad+\mathrm{i}\eta^{-1}\bar{\mathbf{A}}_k\langle \mathrm{e}^{-\mathrm{i}\bar{p}_*^{(k)}\eta(x_3-h_{k-1})}\rangle\bar{\mathbf{q}}_k\\ &\quad+\mathrm{i}\eta^{-1}\mathbf{A}_k\langle \mathrm{e}^{-\mathrm{i}p_*^{(k)}\eta(x_3-h_k)}\rangle\mathbf{q}_k'\\ \tilde{\mathbf{t}}_k(y_1,y_2,x_3)\,\mathrm{e}^{-\mathrm{i}\mathbf{y}\cdot\mathbf{x}^0} &= -\bar{\mathbf{B}}_k\langle \mathrm{e}^{-\mathrm{i}\bar{p}_*^{(k)}\eta(x_3-d)}\rangle\bar{\mathbf{q}}^{\infty}\\ &\quad+\bar{\mathbf{B}}_k\langle \mathrm{e}^{-\mathrm{i}\bar{p}_*^{(k)}\eta(x_3-h_{k-1})}\rangle\bar{\mathbf{q}}_k\\ &\quad+\mathbf{B}_k\langle \mathrm{e}^{-\mathrm{i}p_*^{(k)}\eta(x_3-h_k)}\rangle\mathbf{q}_k'\end{aligned}\tag{9}$$

for $d < x_3 \le h_k$,

where

$$\mathbf{q}^{\infty} = (\mathbf{B}_k\mathbf{A}_k^{-1} - \bar{\mathbf{B}}_k\bar{\mathbf{A}}_k^{-1})^{-1}\mathbf{f}$$

$$\langle \mathrm{e}^{-\mathrm{i}p_*\eta x_3}\rangle = \mathrm{diag}[\mathrm{e}^{-\mathrm{i}p_1\eta x_3}, \mathrm{e}^{-\mathrm{i}p_2\eta x_3}, \mathrm{e}^{-\mathrm{i}p_3\eta x_3}]$$

$$\mathbf{x}^0 = (x_1^0, x_2^0)$$

$$\mathbf{y} = \eta\mathbf{n},\quad \mathbf{n} = \begin{bmatrix} n_1 \\ n_2 \\ 0 \end{bmatrix},\tag{10}$$

where the overbar denotes the complex conjugate; subscript or superscript m and k represent the mth and the kth layer, respectively; n is a unit vector; $\mathbf{A}$ and $\mathbf{B}$ are known 3×3 Stroh matrices; and p_α $(\alpha = 1,2,3)$ the eigenvalues for a given material layer in the transform variable $\mathbf{y}$. It is noted that for the solutions in the source layer k, the first term in Eqs. (8) and (9), proportional to $\mathbf{q}^{\infty}$ or $\bar{\mathbf{q}}^{\infty}$, is the Fourier transform of the infinite Green's function with material property of the source layer. $\bar{\mathbf{q}}_j$ and $\mathbf{q}_j'$ $(j = 1,2,\ldots,n)$ in Eqs. (7)–(9) are complex 3×1 unknown vectors that can be determined from the displacement and traction continuity conditions at each interface, and the traction-free boundary conditions on the top and bottom surfaces:

$$\begin{aligned}&\mathbf{t}_1 = 0, && \text{at } x_3 = 0\\ &\mathbf{u}_1 = \mathbf{u}_2,\ \ \mathbf{t}_1 = \mathbf{t}_2, && \text{at } x_3 = h_1\\ &\vdots && .\\ &\mathbf{u}_{n-1} = \mathbf{u}_n,\ \ \mathbf{t}_{n-1} = \mathbf{t}_n, && \text{at } x_3 = h_{n-1}\\ &\mathbf{t}_n = 0, && \text{at } x_3 = h_n\end{aligned}\tag{11}$$

Note that the conditions

$$\mathbf{u}_k^{(1)} = \mathbf{u}_k^{(2)}, \qquad \mathbf{t}_k^{(1)} - \mathbf{t}_k^{(2)} = \delta(x_1 - x_1^0)\delta(x_2 - x_2^0)\mathbf{f} \ \text{ at } x_3 = d \tag{12}$$

are satisfied by Eqs. (8) and (9). In Eqs. (12), superscripts (1) and (2) denote the regions $h_{k-1} \le x_3 < d$ and $d < x_3 \le h_k$, respectively.

After obtaining Green's functions in the transformed domain, an adaptive quadrature technique is then employed to evaluate physical-domain Green's functions.

4. Treatment of singularity in layered Green's functions

On calculating layered Green's functions using the adaptive quadrature, we found that it is very difficult, if not impossible, to obtain accurate results with the use of numerical integration when the field point is close to the source point (singular point). Since the contribution from the singular point is very critical in the BEM analysis, we propose here a method to evaluate this singular value accurately. First, in the transformed domain, we remove the singularity in layered Green's functions by subtracting them with full-space Green's functions (Green's functions in a homogeneous and infinite space with material property of the source layer). After successfully performing the adaptive integration, full-space Green's functions are then added analytically to layered Green's functions. This approach can be explained clearly in terms of equations.

First, we write the layered Green's displacements, U_{ij}^*, and tractions, T_{ij}^*, as

$$U_{ij}^* = (U_{ij}^* - U_{ij}^{\inf}) + U_{ij}^{\inf} \qquad T_{ij}^* = (T_{ij}^* - T_{ij}^{\inf}) + T_{ij}^{\inf}, \tag{13}$$

where $U_{ij}^{\inf}$ and $T_{ij}^{\inf}$ are the Green's displacements and tractions in a full-space solid with material property of the source layer. These Green's functions can be evaluated very accurately and efficiently by the methods described either by Tonon et al. [29] based on Wang's formulation [30] using Radon transform or by Malen [12] and Ting and Lee [28] using the Stroh formalism. Since in the source layer, layered Green's functions and full-space Green's functions possess the same singularity behavior, the terms in the brackets of Eq. (13) are regular and can, therefore, be evaluated at any point in the source layer. In the double Fourier-transformed domain, Eq. (13) becomes

$$\tilde{U}_{ij}^* = (\tilde{U}_{ij}^* - \tilde{U}_{ij}^{\inf}) + \tilde{U}_{ij}^{\inf} \qquad \tilde{T}_{ij}^* = (\tilde{T}_{ij}^* - \tilde{T}_{ij}^{\inf}) + \tilde{T}_{ij}^{\inf}. \tag{14}$$

As can be observed clearly, for any point belonging to the source layer, our numerical integration is applied to regular functions only, the terms in the brackets in Eq. (14). These non-singular terms actually correspond to the Fourier-transformed Green's functions in Eqs. (8) and (9) without the terms proportional to $\mathbf{q}^\infty$ or $\bar{\mathbf{q}}^\infty$. Applying the adaptive numerical integration to the terms in the brackets in Eq. (14), we obtain non-singular Green's functions in the physical domain, i.e. the terms in the brackets in Eq. (13). Subsequently, full-space Green's functions are superimposed to obtain layered Green's functions in the physical domain, as shown in Eq. (13). Therefore, the handling of singularities in layered Green's functions is transferred to the treatment of singularities in full-space Green's functions. Since the latter functions have explicit expressions, the numerical treatment becomes a trivial task.

5. Calculation of layered Green's functions

Calculation of the aforementioned Green's functions for layered composite structure involves the inverse of the Fourier transform that will be done with an adaptive quadrature (e.g. Ref. [16]). For the transformed-domain Green's displacement, $\tilde{\mathbf{u}}_k(y_1, y_2, x_3)$, in Eq. (6), we apply the inverse of the Fourier transform to obtain

$$\mathbf{u}_k(x_1, x_2, x_3) = \frac{1}{4\pi^2} \int\int \tilde{\mathbf{u}}_k(y_1, y_2, x_3)\, \mathrm{e}^{-\mathrm{i}\mathbf{y}\cdot\mathbf{x}}\, \mathrm{d}y_1\, \mathrm{d}y_2. \tag{15}$$

Expressing the integral variables (y_1,y_2) in terms of polar coordinates (η,θ), we arrive at

$$\mathbf{u}_k(x_1, x_2, x_3) = \frac{1}{4\pi^2} \int_0^{2\pi} \mathrm{d}\theta \int_0^{\infty} \tilde{\mathbf{u}}_k(\eta, \theta, x_3)\, \mathrm{e}^{-\mathrm{i}\eta(x_1 \cos\theta + x_2 \sin\theta)} \eta\, \mathrm{d}\eta. \tag{16}$$

For Green's functions in Eqs. (7)–(9), integration similar to Eq. (16) needs to be carried out for any given pair of d and x_3, where d is the z-coordinate of the source point. It is obvious that repeated and unnecessary calculation of Eq. (16) may be involved if layered Green's functions are called without proper ordering of the boundary coordinates when forming the coefficient matrices in Eqs. (4) and (5). On the other hand, due to the complexity of the problem, a relatively large amount of calculation time is spent on evaluating Fourier-transformed Green's functions (i.e. the first factor of the integrand in Eq. (16) and similar expressions). Therefore, it is necessary to reduce the number of times required for these evaluations to be carried out.

In order to reduce the time for evaluating Fourier-transformed Green's functions (i.e. the first factor of the integrand in Eq. (16)), we examined in detail some features

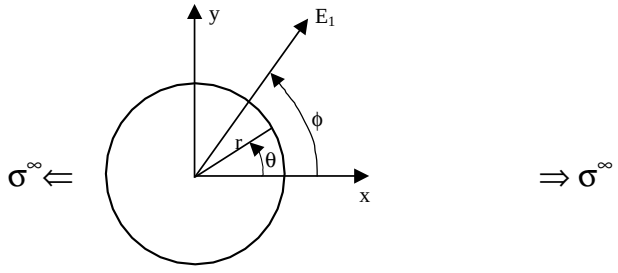

Fig. 2. A circular hole with radius $r = 1$ in an infinite and anisotropic plate under a far-field stress σ^∞ in x-direction.

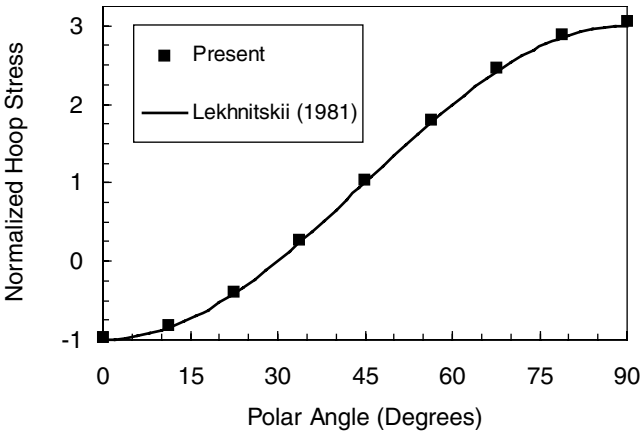

Fig. 3. Variation of the normalized hoop stress $\sigma_{\theta\theta}/\sigma^{\infty}$ along the hole for the isotropic case.

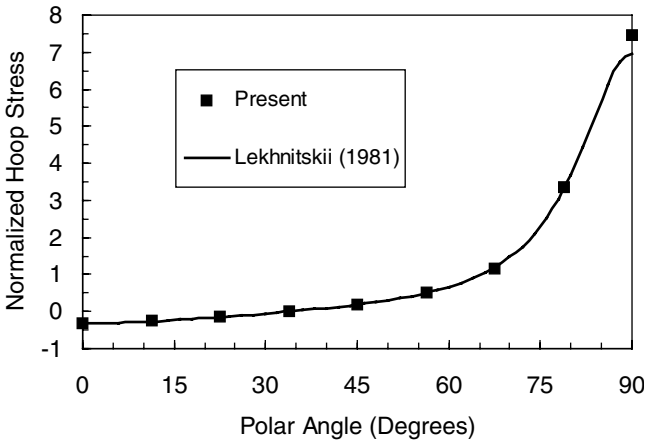

Fig. 4. Variation of the normalized hoop stress $\sigma_{\theta\theta}/\sigma^{\infty}$ along the hole for the anisotropic case with $\phi = 0°$.

associated with these functions. One of the important features is that Fourier-transformed Green's functions depend only upon the vertical coordinates of the source and field points (i.e. d and x_3), not on the horizontal coordinates. Such a feature can, therefore, be utilized when designing the BEM program. The discussion is explained as follows.

First, we order all the boundary nodes properly. For a given vertical coordinate (or a horizontal plane), we find and order all the boundary nodes on this horizontal plane. We then go from this horizontal plane to the next and again order all the corresponding boundary nodes. We repeat this procedure for all the boundary nodes.

Second, we calculate the coefficient matrices in Eqs. (4) and (5). To this end, an outer loop is first performed over all vertical coordinates (i.e. all the horizontal planes) on the boundary. Within this loop, all the nodes on the same horizontal planes (i.e. those nodes having the same pair of d and x_3) are performed. Since this inner loop is executed for the same pair of d and x_3, the Fourier-transformed Green's function, e.g. the first factor of the integrand in Eq. (16), needs to be called only once. In other words, to calculate the physical-domain Green's function (Eq. 16) for a given vertical coordinate pair (and, of course, for the given integral variables η and θ), we need to call only once the Fourier-transformed Green's functions.

The handling of layered Green's functions and the corresponding coefficient matrices in the BEM formulation, based on the adaptive integration approach with suitable boundary node ordering, has been found to be very efficient. It is also more accurate (or the accuracy can be controlled) than the inverse FFT method [2]. Numerical examples given in the next section justified these statements.

6. Numerical examples

In order to test the accuracy and efficiency of layered Green's functions and the corresponding boundary integral equations, the formulations presented above have been implemented and applied to an anisotropic and infinite plate with a

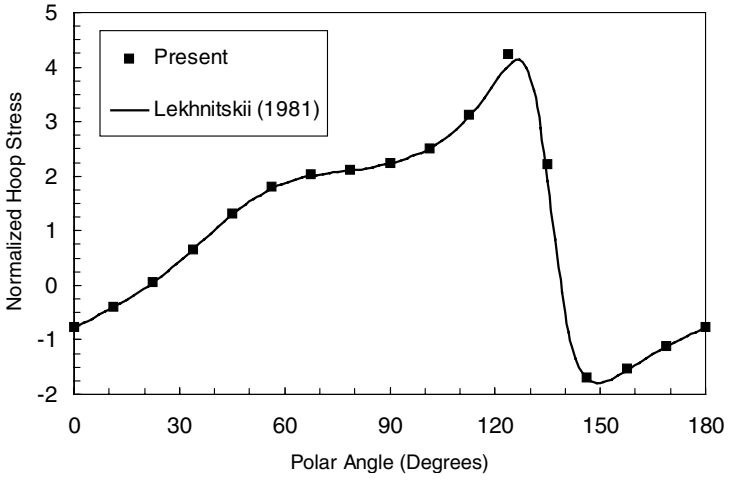

Fig. 5. Variation of the normalized hoop stress $\sigma_{\theta\theta}/\sigma^{\infty}$ along the hole for the anisotropic case with $\phi = 45°$.

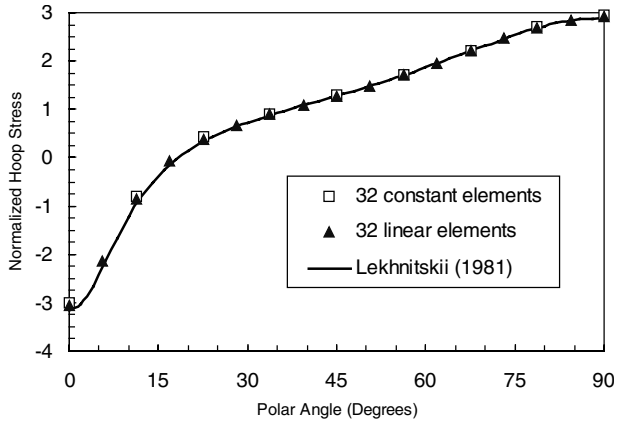

Fig. 6. Variation of the normalized hoop stress $\sigma_{\theta\theta}/\sigma^{\infty}$ along the hole for the anisotropic case with $\phi = 90°$.

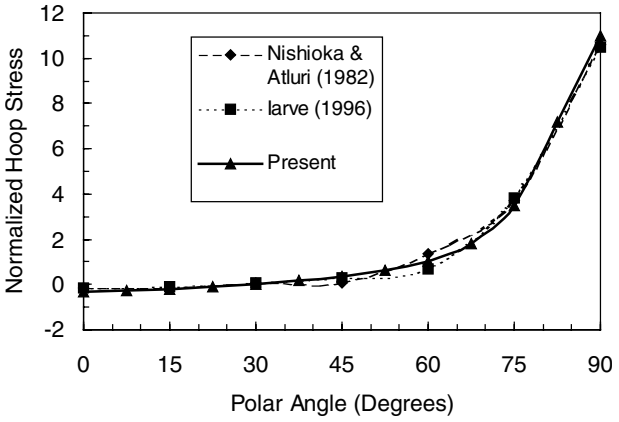

Fig. 8. Normalized hoop stress $\sigma_{\theta\theta}/\sigma^{\infty}$ along the hole in the mid-plane of the 0°-ply ($z = 3h/8$). Four-layered composite laminate $(90/0)_s$.

circular hole. If this plate is subjected to an in-plane uniaxial far-field tension σ^{∞} in the x-direction (Fig. 2), then the exact closed-form solution for the hoop stress along the hole can be found [10]. In our 3D model, we assume that the plate has a thickness of $0.2r$ (i.e. only 1/5 of the radius of the hole) and discretize the hole with constant elements. More specifically, we discretize the hole in the vertical direction with two constant elements and in the circumferential direction with 32 constant elements. Therefore, a total of 64 constant elements (in 3D) are used to discretize the surface of the hole. Numerical results obtained with the present BEM formulation are shown in Figs. 3–6 and are compared to the corresponding exact closed-form solutions [10]. It is shown that even with only 32 constant elements in the circumferential direction, the present numerical results are nearly identical to the exact solutions, with the only exception at the peak of the stress where the numerical results are about 5% larger than the corresponding exact solutions. As for the peak stress, however, a refined mesh or a high-order shape function can be implemented to improve the results. This is observed in Fig. 6 where the use of linear elements with the same node number as for the constant elements has improved the stress value at the peak.

With the layered BEM formulation being tested successfully for the homogeneous plate case, we now apply this formulation to a four-layered symmetric composite laminate. Fig. 7 shows the geometry of an infinite laminated plate with a through-the-thickness circular hole of diameter D. The four orthotropic plies $(90/0)_s$ have equal thickness of $h/4$ each, where $h(= 0.4D)$ is the total thickness of the plate. A uniform far-field strain ε^{∞} is applied in the x-direction. The orthotropic material properties in the material coordinates are selected to be $E_1 = 206.84$ GPa, $E_2 = E_3 = 20.684$ GPa, $G_{13} = G_{23} = G_{12} = 6.895$ GPa, and $\nu_{13} = \nu_{23} = \nu_{12} = 0.336$ [13].

Due to the symmetry of the layered configuration and loading, the BEM model needs to be applied to only half of the layered system (i.e. two plies). Furthermore, using layered Green's functions as the kernel functions in the BEM formulation, we need only to discretize the surface of the hole. For this problem, we discretize in the vertical direction with six constant elements, and in the circumferential direction with 48 and 64 constant elements, respectively, for the $(90/0)_s$ and $(-45/45)_s$ cases. Thus, for the former case, we use totally 288 constant elements only, and for the latter, 384 constant elements only.

The normalized hoop stresses $\sigma_{\theta\theta}/\sigma^{\infty}$ around the hole in the mid-plane of the 0°-ply ($z = 3h/8$) and 90°-ply ($z = h/8$) are shown in Figs. 8 and 9, respectively, with σ^{∞} being the equivalent far-field stress corresponding to the far-field strain θ^{∞}. The results obtained by Nishioka and Atluri [13] using the special-hole-finite elements and by Iarve [8] using the spline variational method are also shown in the figure. It is obvious that the stress distributions predicted by the present layered BEM formulation are in good agreement with those by Nishioka and Atluri [13] and Iarve [8].

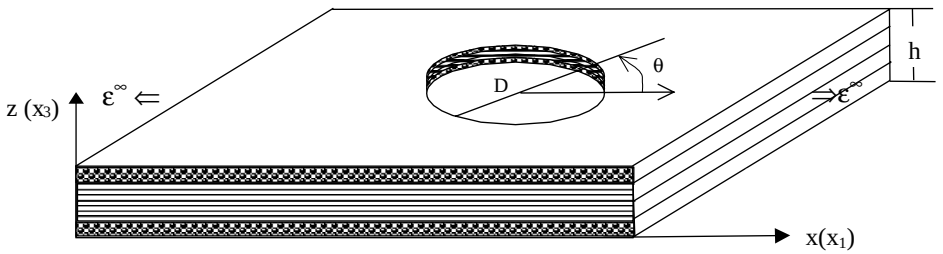

Fig. 7. A four-layered composite laminate $(90/0)_s$ with a central hole under a uniform far-field strain ε^{∞} in the x-direction.

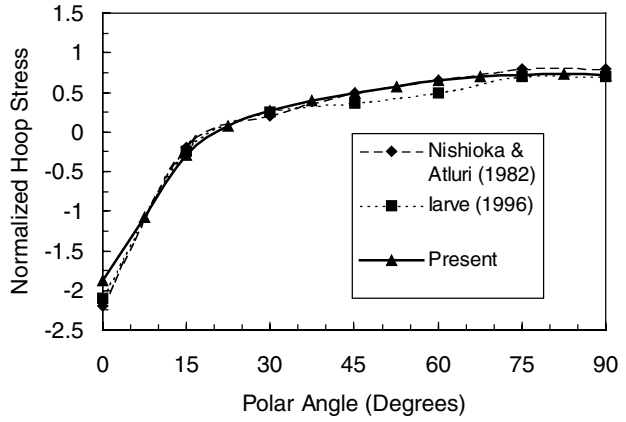

Fig. 9. Normalized hoop stress $\sigma_{\theta\theta}/\sigma^{\infty}$ along the hole in the mid-plane of the 90°-ply ($z = h/8$). Four-layered composite laminate $(90/0)_s$.

However, the stress distributions obtained by the present formulation are much smoother than the previous ones. Furthermore, it is interesting to compare Figs. 8 and 9 with Figs. 4 and 6, respectively. One can easily observe from these figures that while the stress shapes are similar for both the layered and the homogeneous cases, their magnitudes are quite different because of material layering in the former case.

For the four-layered $(-45/45)_s$ composite laminate, the geometry and orthotropic material properties are the same as those for the $(90/0)_s$ composite laminate, except for the ply orientation. Again, as mentioned earlier, totally 384 constant elements are used to discretize the whole surface of the through the thickness hole. Fig. 10 shows the variation of the normalized hoop stress $\sigma_{\theta\theta}/\sigma^{\infty}$ around the hole in the mid-plane ($z = h/2$) of the laminate, as compared to those obtained by Nishioka and Atluri [13] and Rybicki and Hopper [20] using the FEM. It is observed that the stress variation predicted by the present BEM formulation is at great variance with the previous ones. For instance, the location of the maximum stress concentration predicted by the present formulation is approximately at 130°, while the results of Nishioka and Atluri [13], and Rybicki and Hopper [20] are about 120 and 90°, respectively. It is noteworthy that the present result is closer to the exact 2D solution (at 127° in Fig. 5) than the previous results. To justify further the present BEM solution, we have run our BEM program by varying the mesh sizes, and found that the results are consistent with each other and convergent within a less than 5% relative error, as illustrated in Fig. 11.

7. Conclusions

A 3D BEM has been developed for the analysis of composite laminates with holes. 3D layered Green's functions, derived previously by Yuan and Yang [32] in the Fourier transform, have been implemented into the BEM formulation. In order to obtain physical-domain Green's functions, an adaptive quadrature properly connected to the BEM formulation has been proposed. Since layered Green's functions satisfy exactly the interlaminar continuity conditions along the interfaces and top and bottom free surfaces a priori, discretization along these interfaces and surfaces is avoided.

To test the efficiency and accuracy, we applied the present BEM formulation to an analytical case where an anisotropic and infinite plate with a circular hole is under a far-field in-plane stress. It has been shown that even with a very coarse mesh, the hoop stresses along the hole predicted by the present BEM formulation are very close to the analytical solutions.

In order to illustrate the utility of the method, numerical examples were then carried out for two laminates $(90/0)_s$ and $(-45/45)_s$, under a remote uniform in-plane strain. For the $(90/0)_s$ case, the hoop stresses along the hole predicted by the present BEM formulation are in very close agreement with the previous results. For the $(-45/45)_s$ case, however, it is found that a nearly converged solution (less than 5% convergence by doubling the mesh) by the present method is at significant variance with the

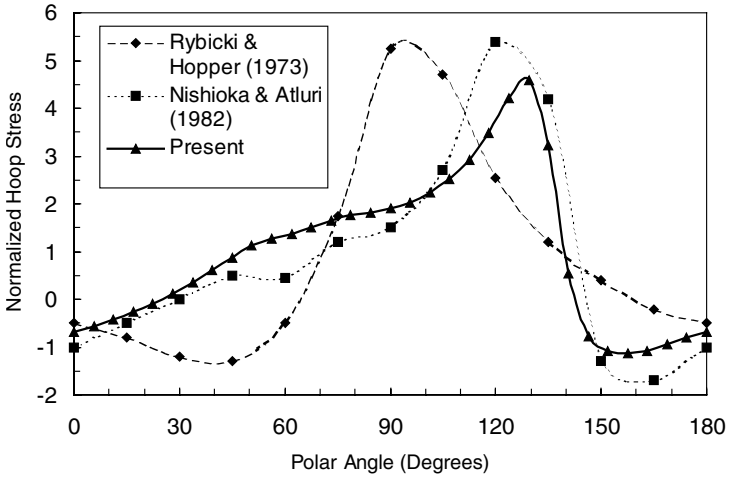

Fig. 10. Normalized hoop stress $\sigma_{\theta\theta}/\sigma^{\infty}$ along the hole in the mid-plane of the composite laminate $(-45/45)_s$ ($z = h/2$).

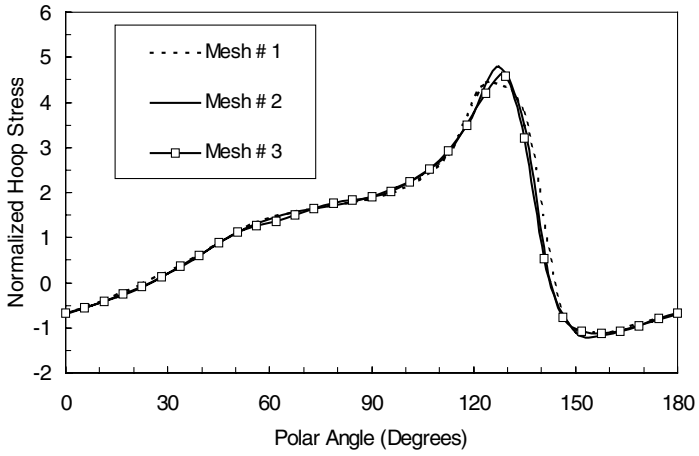

Fig. 11. Normalized hoop stress $\sigma_{\theta\theta}/\sigma^{\infty}$ along the hole in the mid-plane of the composite laminate $(-45/45)_s$ $(z = h/2)$ for three mesh sizes (meshes 1, 2, and 3 are for 32, 64, and 128 constant elements, respectively).

previous ones that are lack-of-convergence checks. The application of such a BEM analysis to layered composite structures with discrete damage is currently under investigation and the results will be reported in a forthcoming paper.

Acknowledgements

The authors are grateful for the support from the Air Force Office of Scientific Research under Grant F33615-97-C-5089, with Dr Richard B. Hall being the project manager. They would also like to thank one of the reviewers for his/her constructive comments.

References

[1] Benitez FG, Lu L, Rosakis AJ. A boundary element formulation based on the three-dimensional elastostatic fundamental solution for the infinite layer: part 1 — theoretical and numerical development. Int J Numer Methods Engng 1993;36:3097–130.
[2] Benitez FG, Wideberg J. The boundary element method based on the three-dimensional elastostatic fundamental solution for the orthotropic multilayered space: application to composite materials. Comput Mech 1996;18:24–45.
[3] Collings TA. On the bearing strengths of CFRP laminates. Composites 1982;13(3):241–52.
[4] De Jong T. Stresses around pin-loaded holes in elastically orthotropic or isotropic plates. J Compos Mater 1977;11:313–31.
[5] DiNicola AJ, Fantle SC. Bearing strength behavior of clearance-fit fastener holes in toughened graphite/epoxy laminates. In: Camponeshi Jr. ET, editor. Composite materials: testing and design, ASTM STP 1206, vol. 11. Philadelphia, PA: American Society for Testing and Materials, 1993. p. 220–37.
[6] Eriksson L. On the bearing strength of bolted graphite/epoxy laminates. J Compos Mater 1990;24:1246–69.
[7] Hart-Smith LJ. The key to designing efficient bolted composite joints. Composites 1994;25(8):835–7.
[8] Iarve EV. Spline variational three dimensional stress analysis of laminated composite plates with open holes. Int J Solids Struct 1996;33(14):2095–118.
[9] Jurf RA, Vinson JR. Failure analysis of bolted joints in composite laminates. In: Garbo SP, editor. Composite materials: testing and design, ASTM STP 1059, vol. 9. Philadelphia, PA: American Society for Testing and Materials, 1990. p. 165–90.
[10] Lekhnitskii SG. Theory of elasticity of an anisotropic elastic body. Moscow: Mir, 1981.
[11] Lubin G. Handbook of composites. New York: Van Nostrand Reinhold, 1982.
[12] Malen K. A unified six-dimensional treatment of elastic Green's functions and dislocations. Phys Status Solidi (B) 1971;44:661–72.
[13] Nishioka T, Atluri SN. Stress analysis of holes in angle-ply laminates: an efficient assumed stress 'special-hole-element' approach and a simple estimation method. Comput Struct 1982; 15(2):135–47.
[14] Pan E. Static Green's functions in multilayered half spaces. Appl Math Modelling 1997;21:509–21.
[15] Pan E, Amadei B. A 3-D boundary element formulation of anisotropic elasticity with gravity. Appl Math Modelling 1996;20:114–20.
[16] Press WH, Flannery BP, Teukolsky SA, Vetterling WT. Numerical recipes. Cambridge: Cambridge University Press, 1989.
[17] Quinn WJ, Matthews FL. The effect of stacking sequence on the pin-bearing strength in glass fibre reinforced plastic. J Compos Mater 1977;11:139–45.
[18] Raju IS, Crews Jr. JH. Three-dimensional analysis of $[0/90]_s$ and $[90/0]_s$ laminates with a central circular hole. Compos Technol Rev 1982;4(4):116–24.
[19] Ramkumar RL, Saether ES, Cheng D. Design guide for bolted joints in composite structures. AFWAL-TR-86-3035, 1986.
[20] Rybicki EF, Hopper AT. Analytical investigation of stress concentration due to holes in fiber reinforced plastic laminated plates: three-dimensional models. AFML-TR-73-100, Battelle Columbus Labs, 1973.
[21] Rybicki EF, Schmuesser DW. Three-dimensional finite element stress analysis of laminated plates containing a circular hole. AFML-TR-76-92, Battelle Columbus Labs, 1976.
[22] Schwartz MM. Composite materials handbook. New York: McGraw-Hill, 1984.
[23] Soni SR. Stress and strength analysis of bolted joints in composite laminates. In: Marshall IH, editor. Composite structures, New York: Applied Science Publishers, 1981. p. 50–62.
[24] Stockdale JH, Matthews FL. The effect of clamping pressure on bolt bearing loads in glass fiber-reinforced plastics. Composites 1976;7:213–25.
[25] Tang S. Interlaminar stresses around circular cutouts in composites plates under tension. AIAA J 1977;15(11):1631–7.
[26] Tang S. A variational approach to edge stresses of circular cutouts in

composites. AIAA Paper 79-0802, 20th AIAA/ASME/ASCE/AHS, SDM Conference, St. Louis, MO, 1979. p. 326–32.
[27] Ting TCT. Anisotropic elasticity. Oxford: Oxford University Press, 1996.
[28] Ting TCT, Lee VG. The three-dimensional elastostatic Green's function for general anisotropic linear elastic solids. Q J Mech Appl Math 1997;50:407–26.
[29] Tonon F, Pan E, Amadei B. Green's functions and boundary element formulation for 3D anisotropic media. Comput Struct 2001;79:469–82.
[30] Wang CY. Elastic fields produced by a point source in solids of general anisotropy. J Engng Math 1997;32:41–52.
[31] Waszczak JP, Cruse TA. Failure mode and strength predictions of anisotropic bolt bearing specimens. J Compos Mater 1971;5: 421–5.
[32] Yuan FG, Yang S. Three-dimensional green's functions for composite laminates and composite half-space. Mech Compos Mater Struct 2001 (in press).